

Enrico Mugnaioli\* and Mauro Gemmi

# Single-crystal analysis of nanodomains by electron diffraction tomography: mineralogy at the order-disorder borderline

<https://doi.org/10.1515/zkri-2017-2130>

Received November 9, 2017; accepted January 2, 2018; published online February 5, 2018

**Abstract:** Electron diffraction tomography is a powerful emerging method for the structure characterization of materials available only as sub-micrometric grains. This technique can in fact deliver complete 3D information from a single crystal of few hundreds or few tens of nanometers, allowing the analysis of polyphasic or polytypic mixtures that generally cannot be fully addressed by X-ray methods. In this paper, we report and discuss three mineralogy-related study cases where electron diffraction tomography was the only way for achieving a proper description of the sample, by the identification and the structure determination of all the phases or all the polytypes within. We also show how electron diffraction tomography and dynamical refinement can be combined for finding accurate atomic positions and localizing hydrogen atoms at room conditions. Finally, we stress the future potential of this method in the fields of mineralogy and experimental petrology, where till now many samples cannot be properly described because nanocrystalline, polyphasic or disordered. Electron diffraction tomography can be used for detecting unexpected or unknown phases in high-pressure synthetic yields or for the characterization of fine rocks formed under extreme conditions, like impactites or meteorites. Eventually, this method allows the structure characterization of single domains that are ordered only at the scale of few cell repetitions, and therefore it makes possible investigating those materials at the borderline between crystalline and amorphous matter and delivers crucial and unique elements for the understanding of the first stages of solid matter organization.

**Keywords:** electron diffraction tomography; experimental petrology; hydrogen atoms; nanomaterials; order-disorder sequences; polytypism.

## Introduction

The discovery that X-ray elastic scattering can be used to determine the periodic atomic arrangement in solid-state matter has greatly modified our view of Nature and materials and may indeed be addressed as one of the major cultural and scientific revolution of the last century. Since then, crystallography significantly contributed to speed the scientific and technological development Human has experienced till nowadays in materials science, solid-state chemistry, physics of matter, pharmaceutical, biology and Earth sciences. Shortly after X-ray diffraction had become a routine technique for atomic structure determination, other short-wavelength radiations, like accelerated neutrons and electrons, were found to be elastically scattered by atoms. In particular, accelerated electrons were soon recognized of two main strengths: (i) they have a Coulomb interaction with matter, which is at least three orders of magnitude stronger than X-ray in terms of scattering amplitude, with obvious advantages for light atoms detection; (ii) they can easily be deflected by electromagnetic lenses and therefore focused in nano-sized probe and/or recombined to form direct-space images, with a resolution orders of magnitude greater than visible light microscopes.

This second aspect has allowed, starting from 1932 [1], the manufacturing of transmission electron microscopes (TEM). Nowadays, after almost one century of engineering developments, TEM can deliver direct-space images with picometric resolution. Still, atomic-resolution images, either obtained in conventional high-resolution transmission electron microscopy (HRTEM) or in high-angular annular dark-field scanning-transmission electron microscopy (HAADF-STEM), normally require an intense illumination of the sample. This high electron dose causes a fast deterioration (radiation damage) of many classes of materials, like organics, biological tissues, water-containing or water-structured materials, porous frameworks.

\*Corresponding author: Enrico Mugnaioli, Center for Nanotechnology Innovation@NEST, Istituto Italiano di Tecnologia, Piazza San Silvestro 12, 56127 Pisa, Italy, E-mail: enrico.mugnaioli@iit.it

Mauro Gemmi: Center for Nanotechnology Innovation@NEST, Istituto Italiano di Tecnologia, Piazza San Silvestro 12, 56127 Pisa, Italy

Additionally, it is not easy to recombine 2D image-like data in a 3D structure-like exhaustive structural information. Finally, the aberrations affecting TEM lenses, and in particular the objective lens, are still major issues that only the latest generation of microscopes has started to deal with.

From the very beginning of electron crystallography [2, 3], some researchers have therefore tried to exploit the diffracted electrons as they are scattered by the sample, without the complication of refocusing them in a direct-space image. The idea of using electron diffraction instead of imaging certainly implies that we have to renounce on the crystallographic phase information, which must be regained later by computational methods, actually the same methods already massively developed for X-ray diffraction. Still, electron diffraction allows for the best resolution possible, it is straightly available in a 3D array and, uppermost, it requires a much milder illumination than imaging, allowing the acquisition of highly complete atomic structure information from almost any material, even if highly beam sensitive.

The fact that accelerated electrons have a stronger interaction with matter compared to X-rays is a decisive factor allowing their ability to deliver structure information for nanoscaled domains. On the other hand, this implies that any material is electron-transparent only when its thickness ranges from some tens (for heavy-metal alloys) to few thousands (for organics and macromolecules) of nanometers. Therefore, powdering or specific cutting or polishing procedures are required for sample investigation. Moreover, even when the sample is electron-transparent, there is a probability, which depends on its thickness and density, that electrons undergo double or even multiple scattering events during sample crossing

[4]. Because reflections are rather broad, due to the small crystal size, and the curvature of the Ewald sphere is rather small, due to the short wavelength of accelerated electrons (0.001–0.004 nm), many reflections are excited at the same time, hence always allowing the condition for multiple scattering.

Double and multiple scattering within the same crystal is normally referred as dynamical effects. The overall outcome of such phenomenon is that intensities are spread among reflections, up to the limit case where all reflections appear to have the same intensity with only a uniform decay related to the scattering angle (Figure 1a). Consequently, dynamical effects break the simple kinematical approximation normally adopted in X-ray diffraction, which states that the intensity of a  $hkl$  reflection is proportional to its squared structure factor amplitude ( $I_{hkl}$  proportional to  $F_{hkl}^2$ ). Dynamical effects may also obliterate axial and plane extinctions, hampering symmetry and space group determination.

A truthful mathematical treatment of dynamical effects is rather complex, involving either a multislice numerical calculation [5] or the Bloch wave analytical treatment [6]. Both methods require anyway a known structural model, or at least a close approximation of it. Simplified or empirical corrections for dynamical effects have also been proposed, but they work only for well-defined experimental settings and under confined assumption, like e.g. the assumption of a simple double scattering phenomenology [7, 8]. In literature, the most common empirical correction is to assume that  $I_{hkl}$  is proportional to  $F_{hkl}$  [9].

The postulation that dynamical effects are unavoidable and garble reflection intensities already for thin samples slowed down development and application of

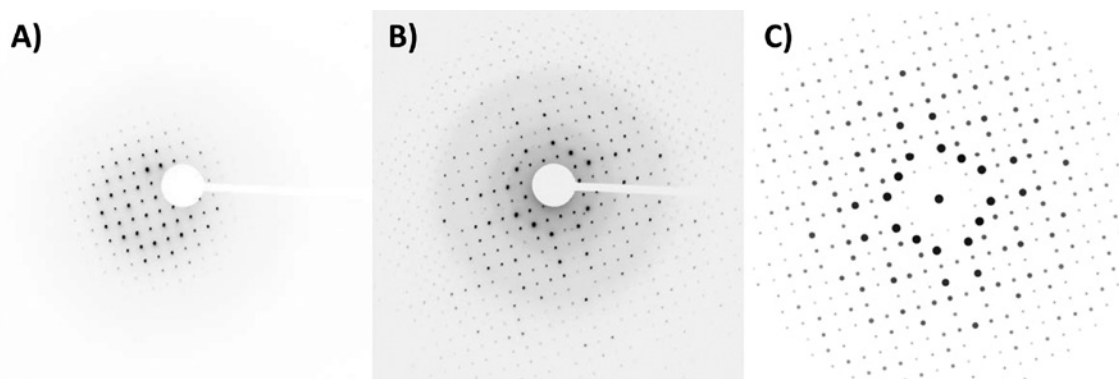


**Fig. 1:** [100] Zone axis pattern of cubic mayenite ( $\text{Ca}_{12}\text{Al}_{14}\text{O}_{33}$ ). (a) SAED pattern. (b) SAED pattern collected with a large precession angle ( $3^\circ$ ). (c) Simulated kinematic pattern. In the SAED pattern, all reflections have very close intensities and the extinctions along the two main axes are not visible. The effect of precession clearly reduces the dynamical scattering as it can be seen by a wider range of the reflection intensities and by the almost disappearance of the odd reflection along ( $h00$ ) and ( $0k0$ ) rows.

quantitative electron diffraction for several decades. Still, in 1950' and 1960' Pinsker [10] and Vainshtein [11] succeeded in manufacturing a dedicated electron diffraction chamber, which allowed collecting structural data from randomly rotated poly-crystalline layered materials, like clays and organics (oblique-texture electron diffraction, OTED). Such data were successfully used for the localization of light atoms, down to hydrogen, and attested the potential of electron diffraction data despite the occurrence of dynamical effects [12].

Only in the late 1970', Dorset demonstrated that it is possible to achieve atomic structure determination on the basis of electron diffraction data recorded in a TEM from a single nanosized crystal or even from a single nanodomain [13, 14]. Later on, Weirich et al. [9, 15] applied standard direct methods developed for X-ray crystallography to solve *ab initio* 2D inorganic structures by a single selected-area electron diffraction (SAED) pattern acquired along a main crystallographic zone axis. Other authors tried to combine more diffraction patterns collected along different low-index crystallographic axes in order to obtain a 3D data set [16–18]. Anyway, this procedure proved little reliable until the advent of the beam-precessed geometry (precession electron diffraction, PED) [19], which allowed for a significant reduction of dynamical effects [20–22] (Figure 1b and c).

Despite the encouraging results obtained by PED, the huge potential of electron diffraction, especially for the emerging fields of nanomaterials and nanotechnologies, was still hampered by the difficulty in acquiring rather complete and pseudo-kinematical data. Additionally, in oriented patterns dynamical effects are emphasized and the time needed for sample orientation may be critical for radiation damage issues.

The key step forward was achieved in 2007, with the introduction by Kolb et al. of a 'tomographic' way of collecting electron diffraction data, initially referred as automated (electron) diffraction tomography (ADT) [23–27], and more recently better known as just electron diffraction tomography (EDT). The main idea behind EDT method is to acquire diffraction patterns neglecting any crystallographic orientation of the sample. Orienting the sample along a low-index crystallographic axis is in fact necessary for obtaining interpretable HRTEM and HAADF-STEM images, but eventually not indispensable, even not desirable, when the aim is a 3D diffraction data set. Off-axis diffraction patterns are then recursively taken while the sample is rotated in fixed angular steps, and the TEM is used as a primitive single-axis diffractometer.

In order to properly integrate the reflection intensities, the Ewald sphere should not be stationary, but rather

integrate over a certain angle in order to reduce or take account of the excitation error (i.e. the distance between the center of a given reflection and the actual position of the Ewald sphere) [28]. This can be achieved either by coupling EDT with PED [25], with a finer rotational step operated by beam tilt (rotation electron diffraction, RED) [29] or with a fast system able to continuously rotate the sample during data acquisition [30, 31].

EDT data collection strategy has three crucial advantages when compared to conventional in-zone patterns:

- (i) The acquisition is easy, reproducible and very fast. Nowadays we can collect more than a 100° tilt series in less than 1 min, acquiring this way quantitative 3D electron diffraction data from extremely beam sensitive materials, like water-containing materials, organics and macromolecules, for which no HRTEM or HAADF-STEM image can normally be recorded at all.
- (ii) All the reflections inside the mechanical limit of the TEM goniometer are sampled, allowing an effortless inclusion of high-index reflections to the data set. In most of TEMs, eventually by using a specifically designed tomographic holder [32], it is possible to rotate the sample in a range of 130° (±65°), resulting in the sampling of a double wedge covering about 2/3 of the reciprocal space. In order to increase the amount of sampled reflections for low-symmetry crystal classes, a second acquisition tilt series can be performed after the sample was rotated in-plane (e.g. of 90°) by a rotational sample holder. In any case, there will be a missing wedge or cone around the vertical axis that cannot be sampled due to mechanical limit [33].
- (iii) The dynamical effects are significantly reduced just because each pattern is collected off-zone, thus decreasing the multiple-scattering probability and the number of unit cell repetitions along the electron beam way. As demonstrated by a number of examples for different classes of materials, in most cases structure determination using EDT data can be achieved by straightly applying the kinematical approximation ( $I_{hkl}$  proportional to  $F_{hkl}^2$ ) [25, 27]. High structural residuals and bad figures of merit are anyway to be expected during the refinement step.

For structures with less than 50 independent atoms and not affected by disorder features, it is also possible to account quantitatively for the dynamical effects by a proper refinement procedure recently developed by Palatinus et al. [34, 35]. This procedure may allow for quantitatively refining partial occupied atom positions and localizing hydrogen atoms in the difference Fourier map [36–39].

## EDT applications to mineralogy and experimental petrology

From the very beginning, EDT found straight way applications in mineralogy and petrology. One of the first new structures determined on the basis of EDT data was charoite-90, still one of the most complex structures (in term of independent atoms in the asymmetric unit) ever solved *ab initio* by electron diffraction data [40] (Table 1). Charoite is indeed a very emblematic case for underlining the potential of EDT. This mineral was well known and clearly recognized since decades, but still no conclusive structure solution could be achieved by conventional X-ray diffraction methods.

Charoite comprises most of the possible troubles that an X-ray crystallographer can meet on his way: (i) charoite crystals never grow in forms suitable for single-crystal X-ray diffraction; (ii) charoite is always associated with other phases, less abundant but generally better crystalline; (iii) charoite forms polymorphs consistent with different order-disorder (OD) arrangements, whose reflections may severely overlap; (iv) charoite cell has relatively long parameters (up to 32 Å) and a large asymmetric unit

with a volume of more than 1000 Å<sup>3</sup> and about 90 independent atoms within; (v) charoite structure is characterized by pseudo-symmetries, that may lead to a wrong crystal system assignment.

As a matter of fact, not even charoite cell parameters and space group could be confidently assigned on the basis of X-ray diffraction. Before the conclusive EDT analysis, the first real insights about charoite structure had in fact come from electron crystallographic methods, i.e. HRTEM imaging and conventional in-zone SAED patterns [41, 42].

The success in solving the long-standing charoite problem has been followed by the structure determination of other hitherto unknown mineral species: charoite-96 [43], sarrabusite [44], widenmannite [45], karibibite [46] and a still unnamed mineral with presumed composition  $(S_{2-1+x}[Bi_{9-x}Te_x(OH)_6O_8(SO_4)_{1/2}]_2$  [47]. EDT also allowed to recover *ab initio* a partial solution for cyanotrichite [48] and kaňkite [49], two very hydrated minerals that grow in assemblies of sub-micrometric domains.

EDT method can sample very small areas, and therefore gives also the unique possibility of acquiring single-crystal structural information from ordered nanoscopic

**Tab. 1:** Structural and experimental details concerning the case studies described in the paper.

Sample	High-temperature Eu <sub>2</sub> Si <sub>2</sub> O <sub>7</sub>	11.5 Å phase	Charoite-90	Charoite-96	Denisovite	Natrolite
Elements (main)	O, Si, Eu	O, Al, Si, Mg	O, F, Si, Na, K, Ca, Sr + water	O, F, Si, Na, K, Ca, Sr + water	O, F, Si, Na, K, Ca + water	O, Al, Si, Na + water
Space group	$P\bar{1}$	$C2/c$	$P2_1/m$	$P2_1/m$	$P2/a$	$Fdd2$
<i>a</i> (Å)	8.5	9.0	32.0	32.1	31.0	18.4
<i>b</i> (Å)	12.9	5.2	19.6	19.8	19.6	18.7
<i>c</i> (Å)	5.3	23.2	7.1	7.2	7.1	6.5
$\alpha$ (°)	91.9	90	90	90	90	90
$\beta$ (°)	87.9	97.8	90.0	95.8	96.0	90
$\gamma$ (°)	90.1	90	90	90	90	90
Cell volume (Å <sup>3</sup> )	580	1080	4450	4560	4310	2240
No. independent atoms (non-H)	22	13	90	87	82	10
TEM type	Zeiss Libra 120		Tecnai F30 S-TWIN		JEOL GEM 2010	Zeiss Libra 120
Acceleration voltage (kV)	120		300		200	120
Diffraction acquisition method	Nano-diffraction (Köhler illumination) and omega filter		Nano-beam diffraction (ADT module)		SAED	Nano-diffraction (Köhler)
Tilt range (°)	95	110	120 + 95 <sup>a</sup>	120 + 110 <sup>a</sup>	110	120
Tilt step (°)	1	1	1	1	1	1
Data resolution (Å)	0.90	0.72	1.15	1.15	1.20	0.80
Indep. data coverage (%)	54	47	97	97	97	91
<i>R</i> <sub>1</sub>	0.292	0.197	0.173	0.339	0.336	0.151 <sup>b</sup>

<sup>a</sup>Data set obtained merging two EDT acquisitions with orthogonal tilt axes from the same crystal; <sup>b</sup>after dynamical refinement.



domains in materials characterized by pervasive disorder or polytypic stacking. This ability was crucial for the recent structure determination of the mineral denisovite [32]. EDT also delivered the hitherto only available *ab initio* structure determination of vaterite [50], whose elusive and thermodynamic unstable configuration produces complex OD polytypic sequences in grains of few tens of nanometers [51, 52]. Additionally, EDT can be used for retrieving 3D structural information from nanocrystalline uncommensurately modulated

materials [53, 54], and might in future be used for the characterization of quasi-crystalline minerals of extra-terrestrial origin [55].

Moreover, linking the 3D diffraction data set with real-space images it is possible to obtain valuable information about grain boundaries, growth mechanisms and geometrical associations in intergrown complexes [56]. Such information can be coupled with the ASTAR technique [57], allowing phase and orientation maps similar to the ones obtained by electron back-scattered diffraction

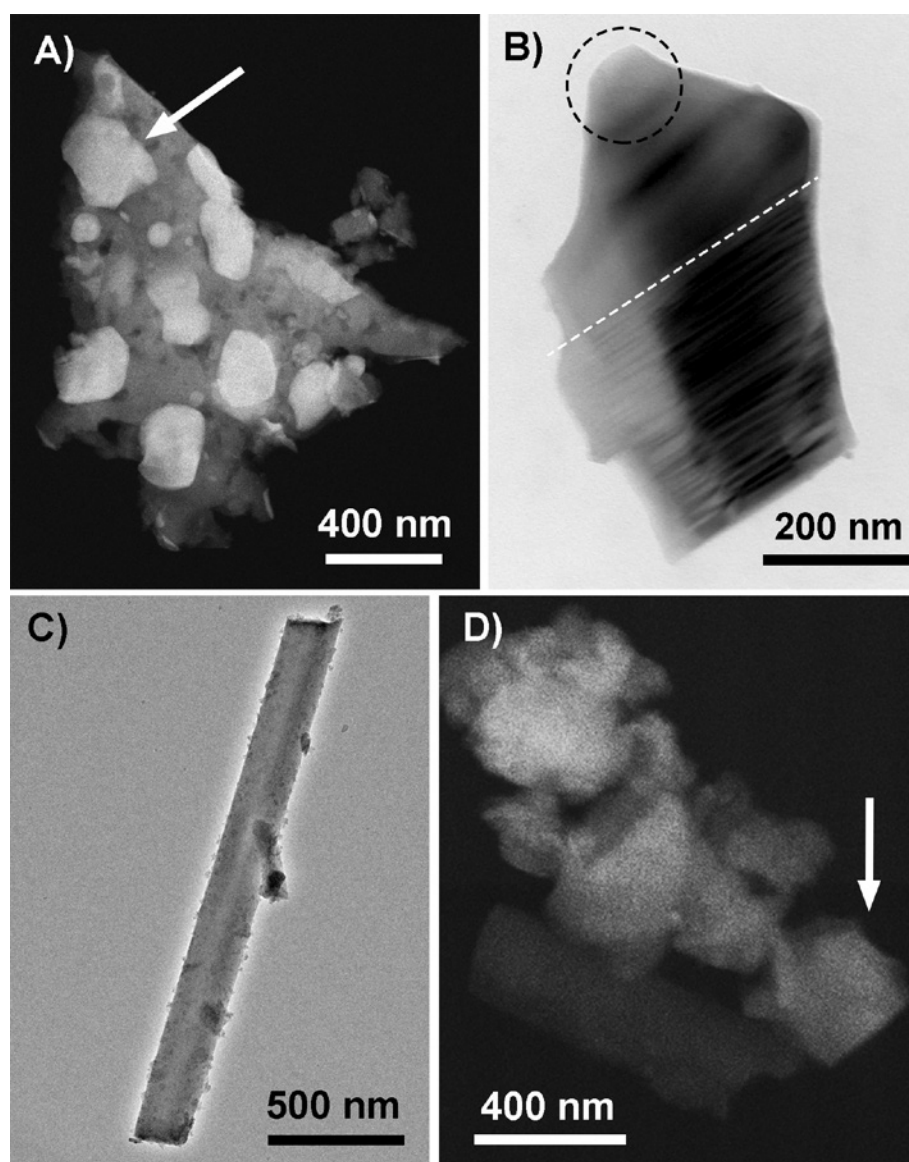


**Fig. 2:** (a) HAADF-STEM image of a shred of Eu-doped silica glass. The bright crystal grains are  $\text{Eu}_2\text{Si}_2\text{O}_7$  embedded in a ground mass of nanocrystalline quartz (darker gray). The EDT data set used for the structure solution was collected from the crystal indicated by the arrow. (b) Bright field image of a crystal grain of 11.5 Å phase, showing fringes of contrast due to stacking disorder at the bottom and a well ordered area at the top. The dashed circle marks the area on which we collected the data for structure solution and has the size of the electron beam. (c) Bright field image of a typical fiber of denisovite. (d) HAADF-STEM image of an aggregate of natrolite crystals. The EDT data set used for the dynamical structure refinement was collected from the crystal indicated by the arrow.

(EBSD), but with one or two orders of magnitude higher point-to-point resolution.

Future EDT applications for mineralogy and petrology look particularly promising in all situations where it is difficult to recover a large amount of material and where the sample is characterized by a high diversity of phases due to non-equilibrated chemical or physical conditions, like e.g. in seismogenic fault mirrors [58], impactitic and meteoritic samples [59], alteration products [60, 61] and yields from high-pressure petrologic experiments [38, 56, 62, 63]. Another interesting application concerns the study of metamict minerals, where EDT allows performing single-crystal analysis of single ordered remains of the supposed original structure, so avoiding the artificial annealing of the sample that is mandatory for X-ray crystallographic studies [64].

In this paper, we will discuss in detail four EDT applications to geology-related problematics (Figure 2 and Table 1). In all these cases, EDT was the only way to achieve a comprehensive *ab initio* crystallographic information because only ordered domains of less than 500 nm were available. In the first chapter, we show the structure characterization of isolated nanometric particles in a matrix-embedded sample: a common case in polyphasic nanocrystalline solid assemblies. In the second chapter, we illustrate how EDT can be used for recognizing and solving unknown phases in a polyphasic high-pressure recovered sample: a case of a hitherto unknown crystal phase determined despite pervasive structural disorder at the nanoscale. In the third chapter, we stress the polytypic recognition in the complex OD stacked assemblies of charoite and denisovite: two cases where polytypic sequences alternate in a scale of few unit cell repetitions. Finally, in the fourth chapter we show how dynamical structure refinement based on EDT data allows obtaining accurate atomic positions, refining partial occupancies and localizing hydrogen atoms for nanocrystalline minerals.

## Materials and methods

### $\text{Eu}_2\text{Si}_2\text{O}_7$

Eu-doped silica samples were obtained by a sintering process of an Eu doped xerogel at 1050 °C for 2 h, followed by a slow cooling. Further details about the synthesis can be found in Baraldi et al. [65].

The TEM sample was obtained by crushing in an agate mortar a small piece of Eu-doped silica sample. The obtained powder was

dispersed in isopropanol and sonicated. After sonication a drop of the dispersion was deposited on a carbon-coated copper grid.

EDT experiments were performed on a Zeiss Libra 120 operating at 120 kV and equipped with  $\text{LaB}_6$  electron source, in-column omega filter for energy filtered imaging and a Nanomegas Digistar P1000 device for precession electron diffraction. Data were recorded in 1° steps with a precession angle of 1°, as described in Mugnaioli et al. [25]. A 5  $\mu\text{m}$  condenser aperture was used in order to have a parallel nanobeam in Köhler illumination with a size of 150 nm. All the patterns have been collected in nano-diffraction mode without selected-area aperture, and the inelastic scattering was filtered out with a 20 eV slit on the zero loss peak. The recording device was a TRS 2k 2k CCD camera.

Data analysis, including 3D diffraction volume reconstruction, cell parameter determination and reflection integration, was performed by PETS software [66]. Structure solution was performed by direct methods implemented in the program SIR2014 [67]. Least squares structure refinement was performed with the software SHELXL [68]. The simple kinematic approximation  $I_{hkl}$  proportional to  $F_{hkl}^2$  was always assumed.

### 11.5 Å Phase

11.5 Å Phase was observed for the first time in a synthesis with Cr-clinochlore bulk composition at 6.5 GPa and 700 °C. The same phase was then resynthesized as majority phase at the same P,T conditions, starting from a bulk composition without Cr, with Mg:Al:Si ratio 5:1:2 and with water in excess. The syntheses were performed on a Walker type multianvil apparatus [69] at the Università degli Studi di Milano, Italy. Further details of the syntheses can be found in Fumagalli et al. [70] and Gemmi et al. [38].

EDT experiments were performed on the same Zeiss Libra 120 and with the same experimental set up as for  $\text{Eu}_2\text{Si}_2\text{O}_7$ . Precession angle was kept at 1°. Data reduction was done by PETS software. Visualization of the 3D diffraction volume reconstruction was performed with the software VESTA [71]. Structure solution was performed by direct methods implemented in the program SIR2014 [67]. Least squares structure refinement was performed with the software JANA2006 [72]. The simple kinematic approximation  $I_{hkl}$  proportional to  $F_{hkl}^2$  was always assumed.

### Charoite

Individual asbestos-like micro-crystals of charoite were obtained crushing and grinding in an agate mortar a light-violet massive specimen. The so-obtained powder was suspended in ethanol and sprayed onto carbon-coated Cu grids using the sonifier described by Mugnaioli et al. [25]. Grids were then mounted on a FISCHIONE tomography holder with a tilt range up to  $\pm 70^\circ$ .

EDT experiments were performed by a Tecnai F30 S-TWIN TEM equipped with field emission gun and operating at 300 kV. Data were recorded in 1° steps using the ADT module described in Kolb et al. [23] and able of routinely switching between  $\mu$ -STEM imaging for crystal tracking and nano-beam electron diffraction for diffraction data acquisition. A 10  $\mu\text{m}$  C2 condenser aperture was used

in order to have a quasi-parallel beam of about 50–70 nm on the sample. Precession electron diffraction was obtained by a NanoMEGAS SpinningStar unit. The precession angle was kept at  $1.0^\circ$  for charoite-90 and  $1.2^\circ$  for charoite-96 data collections, respectively. EDT data were recorded by a Gatan 794MSC CCD camera (14-bit,  $1024 \times 1024$  pixels).

Data reduction was done by ADT3D [26] and in-home developed Matlab routines. *Ab initio* structure determination was achieved by direct methods implemented in the software SIR2008 [73]. Least squares structure refinement was performed with the software SHELXL [68] and CSD [74]. More experimental details are available in Rozhdestvenskaya et al. [40, 43].

### Denisovite

EDT experiments were performed on a JEOL GEM 2010 TEM equipped with  $\text{LaB}_6$  electron source and operating at 200 kV. Crystal position was tracked in standard bright-field imaging mode. Electron diffraction data were acquired in  $1^\circ$  steps in SAED mode from an area of about 150 nm in diameter. Precession electron diffraction was obtained by a NanoMEGAS SpinningStar unit. The precession angle was kept at  $1^\circ$ . EDT data were recorded by an Olympus Tengra CCD camera (14-bit,  $2048 \times 2048$  pixels).

A pure denisovite fiber from Khibini massif was powdered in an agate mortar, dispersed in ethanol and piped onto a carbon-coated copper half-grid. Because the objective lens of the TEM was optimized for HRTEM imaging, a special JEOL EM-21340HTR half-grid specimen retainer was necessary for high-tilt experiments, with a tilt range up to  $\pm 55^\circ$ .

Data reduction was done by ADT3D [26] and in-home developed Matlab routines. *Ab initio* structure determination was achieved by direct methods implemented in the software SIR2014 [67]. Least squares structure refinement was performed with the software SHELXL [68] and CSD [74]. More experimental details are available in Rozhdestvenskaya et al. [32].

### Natrolite

EDT experiments were performed on a Zeiss Libra 120 operating at 120 kV and equipped with a Nanomegas Digistar P1000 device for precession electron diffraction. Data were recorded in  $1^\circ$  steps with a precession angle of  $1^\circ$ . A  $5 \mu\text{m}$  condenser aperture was used in order to have a parallel nanobeam in Köhler illumination with a size of 150 nm. All the patterns have been collected at room temperature in nano-diffraction mode without selected-area aperture and without filtering the inelastic scattering. The recording device was an ASI MEDIPIX detector (14-bit,  $512 \times 512$  pixels).

Data analysis, including 3D diffraction volume reconstruction, cell parameter determination and reflection integration, was performed by PETS software [66]. Structure solution was performed by charge flipping [75] implemented in the program JANA2006 [72]. The structure was refined considering the dynamical effects, as described by Palatinus et al. [34–36]. Refinement parameters were kept at:  $g^{\text{max}} = 1.5 \text{ \AA}^{-1}$ ,  $S_g^{\text{max}}(\text{matrix}) = 0.01$ ,  $S_g^{\text{max}}(\text{refine}) = 0.1$ ,  $R_{\text{sg}} = 0.4$ ,  $N_{\text{steps}} = 64$  (see references [35] and [36] for the explanation of each parameter). Fourier maps were visualized by the software VESTA [71].

## Results and discussion

### Phase mixture at the nanoscale: $\text{Eu}_2\text{Si}_2\text{O}_7$

This first example of EDT application to a difficult and apparently unsolvable crystallographic problem comes from materials science, but can be easily translated into a geologic context assuming we have an exsolution of crystal phases at the nanometric scale. The basic question concerned the identification of the phases forming during the devitrification process of a Eu-doped silica glass. In Eu-doped silica samples sintered at high temperature and slowly cooled down, we observed an inhomogeneous crystallization of Eu-rich nanoparticles that in different area of the sample can be either small (30–70 nm) and surrounded by an amorphous matrix, or large (100–500 nm) and embedded in a nanocrystalline quartz matrix (Figure 2a). The nature of the small nanoparticles could be easily determined as  $\text{Eu}_5(\text{SiO}_4)_3\text{O}$  by indexing a powder electron diffraction pattern collected on an aggregate. The same method could not be applied to the larger particles due to the presence of diffraction peaks belonging to quartz and to the incompleteness of the diffracted rings caused by the larger particle size. However, the presence of only  $\text{Eu}_5(\text{SiO}_4)_3\text{O}$  and quartz could not satisfactorily explain the spectroscopy measurements, which called for the presence of an Eu sorosilicate [65].

The available beam size for an EDT experiment fell nicely in the size range of the large particles, therefore each of them could be studied as a single crystal. The selected candidate can be seen at the top right of Figure 2a: a nanoparticle of 400 nm emerging from the edge of a sample shred. The EDT experiment covering a tilt range of  $95^\circ$  delivered a triclinic unit cell with  $a = 8.50(7) \text{ \AA}$ ,  $b = 12.9(1) \text{ \AA}$ ,  $c = 5.32(5) \text{ \AA}$ ,  $\alpha = 91.9(5)^\circ$ ,  $\beta = 87.9(5)^\circ$ ,  $\gamma = 90.1(5)^\circ$ . This unit cell is in good agreement with the high temperature form of  $\text{Eu}_2\text{Si}_2\text{O}_7$  reported by Felsche [76], whose crystal structure, eventually never solved, was assumed to be related with the high temperature form of  $\text{Sm}_2\text{Si}_2\text{O}_7$ , later determined by single-crystal X-ray diffraction by Christensen et al. [77] in space group  $P\bar{1}$  (Figure 3a).

Structure solution by direct methods based on EDT data in the same space group delivered in fact a structural model very similar to the expected one (Table 1). All the atom positions were found *ab initio* by direct methods and later refined by least squares imposing soft restraints on Si–O distances (Figure 3b). The related cif file is available as Supporting Information.  $\text{Eu}_2\text{Si}_2\text{O}_7$  crystal structure is formed by a 3D network of edge and corner sharing seven-fold and eight-fold Eu–O polyhedra, which forms



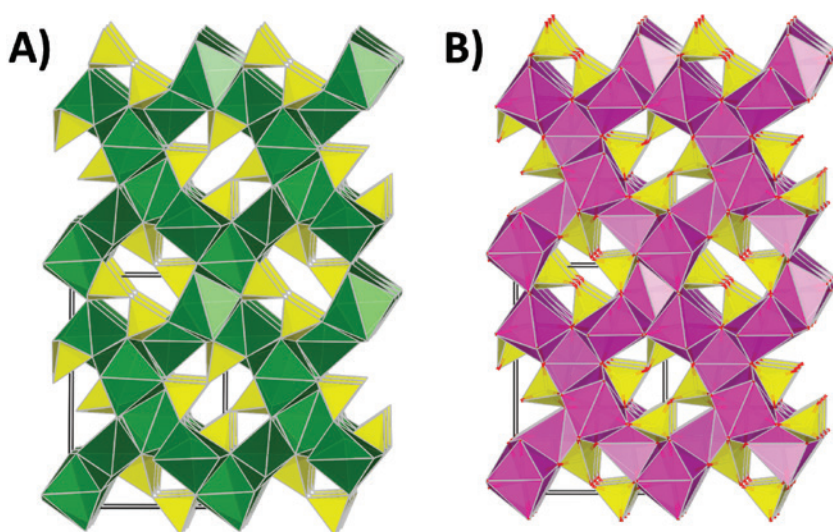


**Fig. 3:** (a)  $\text{Sm}_2\text{Si}_2\text{O}_7$  structure determined by Christensen et al. [77] on the basis of single-crystal X-ray diffraction and (b)  $\text{Eu}_2\text{Si}_2\text{O}_7$  structure determined in this study on the basis of EDT data. Both structures are viewed on a direction close to  $[001]$ .  $\text{SiO}_4$  tetrahedra are represented in yellow,  $\text{SmO}$  polyhedra in dark green,  $\text{EuO}$  polyhedra in violet, O atoms in red.

two crystallographically independent and rectangularly shaped channels along the  $c$  direction. One crystallographically independent  $\text{Si}_2\text{O}_7$  group is located inside each channel, stretching across the channels axis, along directions  $[120]$  and  $[-120]$ , respectively. Each  $\text{Si}_2\text{O}_7$  group has an alternated setting along  $c$  and share all six external oxygens with the  $\text{Eu}-\text{O}$  network.

The result obtained for high-temperature  $\text{Eu}_2\text{Si}_2\text{O}_7$  is remarkable because it demonstrates that a crystal structure that contains both heavy and light atoms can be solved on the basis of EDT data collected on a single nanoparticle of few hundreds of nanometers embedded in a nanocrystalline matrix, whereas the same structure type could not be solved *ab initio* by X-ray powder diffraction on a pure powder sample (see Christensen et al. [77] for the  $\text{Sm}_2\text{Si}_2\text{O}_7$  case). The structure determination of  $\text{Eu}_2\text{Si}_2\text{O}_7$  completes the description of the material formed during the devitrification of Eu-doped silica glasses and allows the thorough interpretation of the spectroscopic measurements on bulk sample.

### Order-disorder at the nanoscale: 11.5 Å phase

High-pressure high-temperature experiments are natural training grounds for the EDT method. A typical sample consists of a few cubic millimeters collection of several crystal species. The extreme crystallization conditions do not allow to grow large single crystals: most grains

are below one micron and some phases show defect features due to their slow kinetics of crystallization. Powder diffraction experiments are the only option for X-ray and neutron radiations. However, the small amount of sample and its polyphasic nature make the powder approach always challenging, especially if unknown phases are present. EDT, instead, is a single-crystal technique, and as such it cannot give a global view of the sample, but is the perfect tool for hunting unknown crystal phases among sub-micrometric crystal grains.

A typical EDT search starts if the powder diffraction analysis cannot be interpreted assuming only known or expected phases, and some diffraction peaks remain unexplained. Then, a dispersion of the sample on a carbon-coated grid is carefully searched at the TEM and each crystal grain is chemically checked by energy dispersive X-ray (EDX) spectroscopy and crystallographically checked by the recently developed fast-EDT method [31]. In this way, we can have at the same time a rough estimate about the chemical composition and the unit cell of a large number of grains, which allow a fast discrimination between known phases and problematic grains. The latter are further investigated via complete EDT data collections, which eventually can provide *ab initio* structure determination. This workflow has been successfully applied to the identification and characterization of three new high-pressure phases: HAPY [62], HYSO and the 11.5 Å phase [38]. Remarkably HYSO and 11.5 Å phase were discovered in the same experiment, a chlorite bulk composition at 6.5 GPa and 700 °C.



The solution of the 11.5 Å phase is particularly challenging since, for its layered nature, this phase is usually disordered and the streaking connected to the random stacking of layers is so severe that even the unit cell parameters cannot be easily determined by EDT measurements (Figure 4a). The 11.5 Å phase has a Mg:Al:Si ratio of 6:1:2 and, perpendicularly to the stacking, its structure exhibits a projected centered rectangular cell with  $a = 8.9$  Å and  $b = 5.1$  Å, which is characteristic of phyllosilicate building blocks. Apart from this, nothing more can be said about its crystal structure by an EDT experiment performed on most of the grains.

Ordered domains of few hundreds of nanometers can be found on rare crystal grains always in association with completely disordered areas. Luckily, the disordered portions can be easily imaged as alternating dark and bright contrast lines in bright-field images (Figure 2b), thus a

large number of candidate grains can be screened-out searching for large coherent regions. A complete EDT data collection could be eventually performed on a single ordered domain avoiding streaking in the diffraction patterns. From this data set it was possible to determine the unit cell, the symmetry, and the crystal structure of an ordered polytype of the phase.

Ordered 11.5 Å phase crystallizes in a *C*-centered monoclinic unit cell, with parameters  $a = 9.012(1)$  Å,  $b = 5.201(1)$  Å,  $c = 23.202(5)$  Å,  $\beta = 97.8(1)^\circ$  and space group *C2/c* (Figure 4b–d and Table 1). The structure solution obtained *ab initio* with direct methods and refined in kinematical approximation with JANA2006 confirms that the structure is a layered silicate with a previously unknown topology [38] (Figure 5). It is built by the alternation of T–O–T blocks, with the T-layers formed by isolated  $\text{SiO}_4$  tetrahedra, and O–O blocks of face sharing tri-octahedral

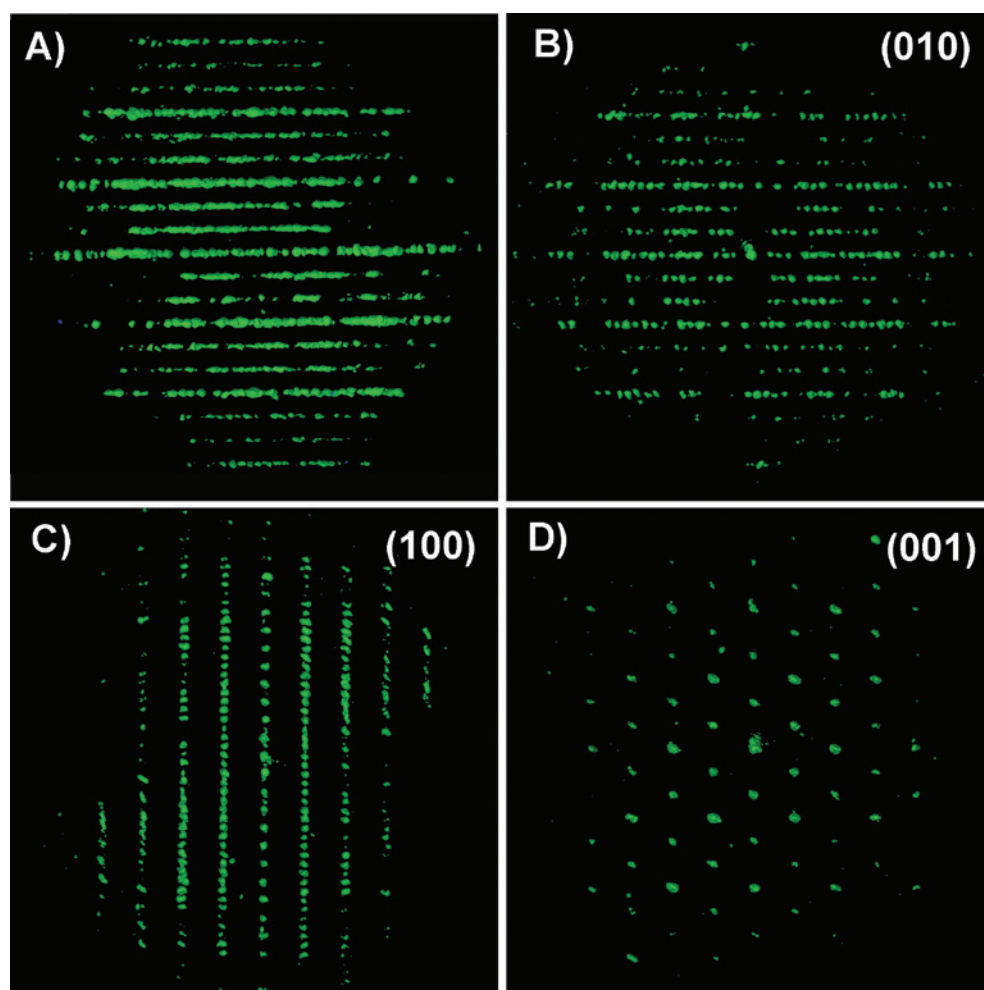


**Fig. 4:** Projections along main reciprocal directions of the 3D reconstructed diffraction volume of 11.5 Å phase. (a) Projection along (010) of a disordered area. (b) Projection along (010) of the ordered phase. (c) Projection along (100) of the ordered phase. Extinctions related with the *c* glide plane are clearly visible. (d) Projection along (001) of the ordered phase. The centered rectangular pattern is due to the *C*-centering.

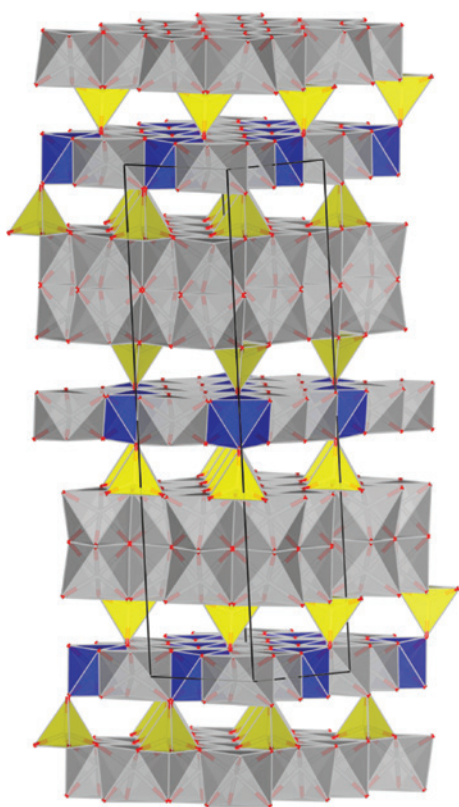


**Fig. 5:** The structure of 11.5 Å phase as determined by Gemmi et al. [38], viewed along a direction close to [110].  $\text{SiO}_4$  tetrahedra are represented in yellow,  $\text{AlO}_6$  octahedra in blue,  $\text{MgO}_6$  octahedra in gray, O atoms in red.

layers. A unit cell is formed by an ordered double sequence of T–O–T/O–O, which mimics a  $2M_2$  polytype of layer silicates. The disordered polytypes arise when the stacking is random, as it typically happens in disordered micas. The chemical formula derived considering electro-neutrality and cation ordering on the octahedral sites is  $\text{Mg}_6\text{Al}(\text{OH})_7(\text{SiO}_4)_2$ , which perfectly fits with the observed Mg:Al:Si ratio and also reveals a high water content as expected from microprobe measurements.

It is noteworthy that in this investigation many key points could be addressed only by the EDT method. By starting with a challenging X-ray powder pattern and some problematic microprobe analyses, EDT revealed two new crystal phases (HYSO and 11.5 Å phase) and allowed determining *ab initio* their crystal structures. For the 11.5 Å phase, the elucidation of the crystal structure of the ordered polytype allowed recognizing the mechanism responsible for the disorder and deriving the complete chemical formula. In turn, this formula confirms the presence of water in the structure, with very interesting implications for the petrology of subduction zones.

## Polytypic and polysomatic analysis at the nanoscale: charoite and denisovite

Charoite,  $(\text{K},\text{Sr})_{15-16}(\text{Ca},\text{Na})_{32}[(\text{Si}_{70}(\text{O},\text{OH})_{180})](\text{OH},\text{F})_{40} \cdot n\text{H}_2\text{O}$ , and denisovite,  $\text{K}_{14}\text{Ca}_{42}\text{Na}_6[\text{Si}_{60}(\text{O},\text{OH})_{162}]\text{F}_{16}(\text{O},\text{OH})_8 \cdot 2\text{H}_2\text{O}$ , are two relatively rare fibrous silicate minerals outcropping in few localities in Russia. Charoite occurs only in the Murum massif, Sakha Republic, and it is excavated and commercialized as a valuable semi-precious stone because of its typical violet color. Denisovite forms grayish aggregates of tiny fibers and has been reported both in the Khibini massif, Murmansk Region, and in the Murum massif. Charoite was firstly described as canasite and later officially accepted as a new mineral in 1978 [78], while denisovite was recognized shortly after in 1984 [79]. The crystal structures of both minerals have remained a puzzle for more than 40 years, both because it was not possible to isolate single crystals suitable for X-ray diffraction, and because powder data could not deliver conclusive answers even about their cell parameters and symmetry.

Indeed, several factors hamper the structure investigation of these two minerals by powder data. First, it is very difficult to isolate a pure charoite sample, that normally is finely intergrown with other more crystalline minerals. Then, both charoite and denisovite have large cell parameters (Table 1), which imply a strong peak overlap at medium-high resolution, worsened by the considerable peak broadening due to the small and strongly anisotropic crystal habit. Finally, both minerals were recently found to form OD polytypes, where different maximum degree of order (MDO) sequences alternate to more disordered segments, all inside what in optical microscopy may look like a single micrometric fiber (Figure 2c). OD polytypes have closely commensurate cells, and it may happen that metrically orthorhombic lattices conceal in fact a monoclinic symmetry. The overall result is a systematic or pseudo-systematic overlap of symmetrically independent reflections in the powder pattern.

Not by chance, the first substantial insights about charoite structure followed from HRTEM imaging and conventional in-zone electron diffraction, i.e. from crystallographic techniques able of a high spatial resolution, that eventually allowed discriminating the single ordered domains. Two ‘more ordered’ polytypes were recognized by conventional in-zone SAED [42] (Table 1). Because the main difference between the two lattices involved the  $\beta$  angle value (of about  $90^\circ$  and  $96^\circ$ , respectively), the two polytypes were named charoite-90 and charoite-96. The first structural model for charoite-96 was derived by a single 2D HRTEM image taken along the short *c* axis and by previous knowledge about related tubular minerals

[41]. The difficulty in orienting charoite structure along the two long axes  $a$  and  $b$  and in interpreting these projections in terms of overlapping atoms, prevented anyway to get a flawless 3D model.

*Ab initio* structure determination of charoite structure was finally achieved on the basis of EDT data collected from an ordered fiber about 150 nm thick and consisting of only charoite-90 [40]. Any structure solution attempted in orthorhombic space group failed despite the apparent orthogonal lattice. On the contrary, direct methods converged immediately when symmetry was reduced to the monoclinic space group  $P2_1/m$ , allowing for a final residual  $R_1$  of 0.173. All 79 independent atoms composing charoite framework were determined directly by direct methods or revealed by the first difference Fourier map. Further refinement allowed the localization of the main ion and water molecule positions inside the channels (Figure 6a and b).

After the determination of charoite-90 structure, Merlino proposed to describe the whole charoite polytypic system in terms of OD sequences (see his Appendix to Rozhdestvenskaya et al. [40] for specific details and Dornberger-Schiff and Fichtner [80] and Ferraris et al.

[81] for a general explanation of OD theory and related symmetry formalism). The basic units of charoite are layers ( $a/2$ ,  $b$ ,  $c$ ), with layer group symmetry  $P(2)mm$ . Such layers are stacked according with the groupoid symbol:

$$P \quad \begin{matrix} (2) \\ \{ (n_{1,1/2}) \\ \{ (n_{1,1/2}) \end{matrix} \quad \begin{matrix} m \\ 2_1 \\ 2_1 \end{matrix} \quad \begin{matrix} m \\ 2_{1/2} \\ 2_{1/2} \end{matrix} \quad \begin{matrix} \\ \} \\ \} \end{matrix}$$

In particular,  $2_{1/2}$  represents a two-fold screw axis with  $1/4$  translation component along  $c$ .

Due to the mirror plane orthogonal to  $c$ , operations  $2_{1/2}$  and  $2_{-1/2}$  produce geometrically equivalent pairs of layers. Therefore, two MDO sequences are in fact possible. The first one, with alternating  $2_{1/2}$  and  $2_{-1/2}$ , would correspond to the *ab initio* experimentally determined charoite-90 structure. The second one, with only  $2_{1/2}$  (or equivalently only  $2_{-1/2}$ ), would correspond to a hypothetical model for charoite-96.

Merlino's proposal was very soon confirmed by the *ab initio* structure solution of charoite-96, again based on EDT data [43] (Figure 6c). In this case, data collection was further complicated by the fact that charoite-96 domains

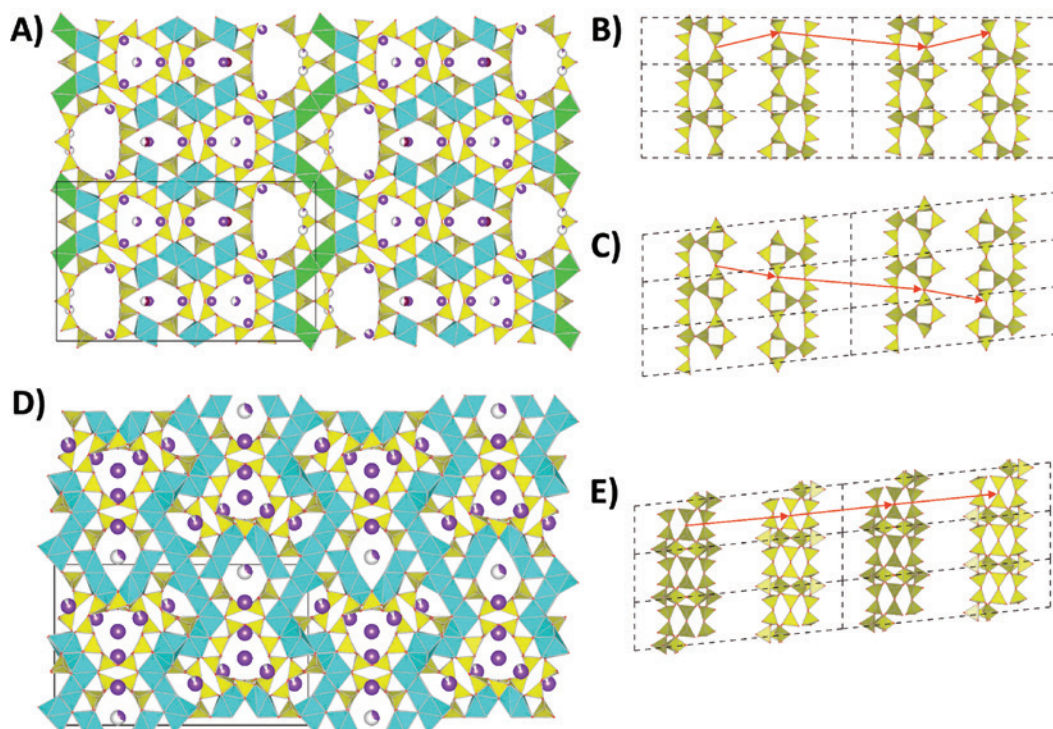


**Fig. 6:** Charoite-90 structure [40] viewed along [001] (a) and along [010] (b), charoite-96 structure [43] viewed along [010] (c) and denisovite structure [32] viewed along [001] (d) and [010] (e). In the [010] views, only the tubular loop-branched dreier triple chain  $[\text{Si}_{12}\text{O}_{30}]^{12-}$  is represented. Red arrows mark the stacking vector connecting succeeding basic layers ( $a/2$ ,  $b$ ,  $c$ ).  $\text{SiO}_4$  tetrahedra are represented in yellow,  $\text{NaO}_6$  octahedra in green,  $\text{CaO}_6$  octahedra in light blue, O atoms in red, F atoms in light gray, K atoms in purple, Sr atoms in dark red. For K and Sr partial occupancy is also shown.



were generally smaller and always associated with charoite-90 or disordered sequences in the same micrometric fiber.

Very similar problems were faced for the recent structure determination of denisovite [32]. This mineral has cell parameters remarkably similar to charoite (Table 1) and therefore for a long time the idea that the two structures were closely related was commonly accepted. Again, the first sound hints about denisovite structure came from electron microscopy and conventional in-zone electron diffraction. SAED patterns showed that denisovite is characterized by a prominent diffuse scattering along  $\mathbf{a}^*$  for reflection lines  $hkl$  with  $l \neq 2n$ , evidence of a pervasive disorder along this direction. Coherent domains are generally smaller than 100 nm, and nano-beam electron diffraction patterns taken from such areas allowed defining a monoclinic lattice (Table 1), with extinction symbols  $P1a1$  or  $P1n1$ . HAADF-STEM images taken along the short lattice direction  $\mathbf{c}$  eventually displayed a completely different framework topology than charoite.

After an extensive search, it was finally possible to acquire sufficiently complete and reliable EDT data sets from three mostly ordered domains of about 200 nm in size. These data allowed the *ab initio* structure determination of denisovite in space group  $P2_1/a$  (Figure 6d and e). As expected, denisovite has a significantly different framework in respect to charoite, but again its structure and stacking can be described in terms of OD sequences. Layers ( $a/2$ ,  $b$ ,  $c$ ) with symmetry  $P(m)2m$  are stacked with groupoid symbol:

$$\begin{array}{ccccccc} P & & (m) & 2 & & m & \\ & \{ & (2_2) & n_{1/2,1} & & 2_{1/2} & \} \end{array}$$

Like for charoite, two MDO sequences are possible. The one with only  $2_{1/2}$  actually corresponds to the experimentally determined structure on the basis of EDT data, and can therefore be labeled as denisovite-96. The one with alternating  $2_{1/2}$  and  $2_{-1/2}$  would correspond to a hypothetical polytype denisovite-90 with space group  $P2_1/m11$ , never observed in a coherent repetition of a substantial number of unit cells. The rather not systematic occurrence of  $2_{1/2}$  and  $2_{-1/2}$  along  $\mathbf{a}^*$  determines the alternation of different polytypic sequences, twinning and stacking faults at the scale of few unit cells [32].

It is worth mentioning that both charoite and denisovite are ranked among the 1% most complex mineral structures known to date, according to a recent complexity parameter proposed by Krivovichev (2013) and based on information theory [82]. Though, it was possible to characterize their MDO polytypes and describe their stacking sequences even when these alternate in a range

of few hundreds or few tens of nanometers, i.e. less than 100 unit cell repetitions for charoite and probably about 20–30 cell repetitions for denisovite.

We want finally to stress that for charoite-96 and denisovite it was not possible to acquire a full EDT data set from a completely coherent ordered domain. Therefore, it is not surprising that the final structural residuals were considerably high, respectively  $R_1$  of 0.339 for charoite-96 and 0.336 for denisovite. This high residual can be only partially ascribed to dynamical effects, but it is rather the consequence of a high fraction of not coherent areas in the sampled diffracting volume. Anyhow, at present EDT looks like the only crystallographic technique able to retrieve a structure from a stack of few coherent unit cells. Still, as for other highly disordered polytypic materials, like e.g. vaterite ( $\text{CaCO}_3$ ) [50], the structures of charoite and denisovite must be considered as ‘most common’ or ‘most probable’ sequences, whose disclosure is anyway necessary in order to understand the mechanisms regulating their polysomatic arrangements.

### Accurate atomic coordinate determination and hydrogen localization by dynamical refinement: natrolite

The number of structures solved on the basis of EDT data using the simple kinematic approach exhaustively demonstrates that dynamical effects can be in general neglected for *ab initio* structure determination. Nevertheless, structural residuals generally associated with standard kinematic refinements are significantly higher than the ones typical of X-ray crystallography. Additionally, errors of tens of picometers must be expected in atom coordinates and interatomic distances, and partial occupancies and displacement factors normally cannot be properly defined [36].

Since 2013, Palatinus et al. [34] have developed a suite of routines able to perform least squares refinement modeling dynamical effects with Bloch wave theory. Structural residuals associated with this kind of refinement are significantly reduced, down to values comparable with X-ray crystallography [83]. More important, it has been demonstrated that structure refined with the dynamical approach are generally more reliable, allowing discriminating between different possible symmetries [84], obtaining reliable geometry of coordination [85], discriminating between atomic species with similar atomic scattering [86] and between different oxidation state of the same element [87], localizing hydrogen atoms, even in beam sensitive and partially disordered materials [39].



Dynamical refinement has already been successfully applied to mineralogy. Jacob et al. [37], on the basis of a single SAED pattern, and Palatinus et al. [36], on the basis of a full EDT tilt series, refined the ratios Mg:Fe in two partially occupied sites of an orthopyroxene. This information, retrieved from areas of few hundreds or tens of nanometers, can be used as a geospeedometer for reconstructing the temperature path during mineral formation. Gemmi et al. [38] used dynamical refinement for localizing partially occupied atomic positions in the synthetic HP phase HySo. This allows the accurate quantification of the water carried by this phase in the upper mantle and at the same time suggests a smooth water vs. MgO substitution process.

Looking for further applications of dynamical refinement in Earth sciences, we tested the sensitivity of the method for the localization of hydrogen atoms in minerals. We therefore acquired an EDT data set from a single squared crystal of natrolite of about 200 nm in size (Figure 1d). Natrolite is a relatively simple natural zeolite with a single water molecule in the channel. Based on these data, natrolite structure was solved *ab initio* by charge flipping implemented in JANA2006 [72, 75]. All atoms beside hydrogen ones were correctly localized. Kinematic refinement of the *ab initio* model did not lead to any significant improvement and converged with a residual  $R_{\text{obs}}$  of 0.219.

Subsequently, data were treated according to dynamical theory, refining in a first step only the experimental parameters: sample thickness, individual scale and fine orientation of each pattern. The resulting difference Fourier map already showed two well defined maxima corresponding to the expected positions of the hydrogen atoms. The water molecule lay flat orthogonal to an ideal Na–Na axis, about at the same distance from the two Na atoms. O–H distances were respectively 1.10 Å and 1.29 Å (Figure 7). The dynamical refinement of the structure converged with a residual  $R_1$  of 0.151, after imposing soft restraints only on O–H distances. Interestingly, the angle H–O–H refined without geometrical restraint to a value of 106.7°, quite close to the expected value of 109.5°. Finally, it is also remarkable to mention that Al and Si positions could be easily distinguished on the basis of the well-defined Si–O and Al–O distance ranges, of 1.60–1.65 Å and 1.70–1.77 Å respectively. The cif file of the final refined structure is available as Supporting Information.

The result obtained for natrolite is quite fascinating, considering that hydrogen atoms belonged to a relatively free water molecule, the material was not deuterated, the experiment was performed at room temperature and in vacuum, data were collected by a relatively affordable 120 kV TEM which does not require a dedicate large-scale

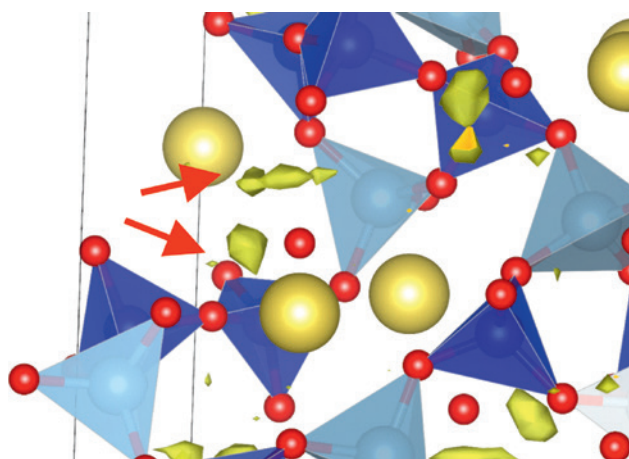


**Fig. 7:** Natrolite structure determined *ab initio* by charge flipping with a kinematical treatment of EDT data, superimposed to the difference Fourier map calculated with a dynamical treatment after a preliminary refinement of the experimental parameters (sample thickness, scale and fine orientation of each diffraction pattern). Red arrows point the two potential peaks corresponding to the missing hydrogen atoms of the water molecule. Si and Al atoms are represented inside their tetrahedra of coordination (in blue and gray, respectively). O atoms are in red, Na atoms are in yellow.

facility and also allows for low-temperature and high-temperature experiments.

## Conclusions and perspectives

We believe that EDT method has huge potential for the determination of hitherto unknown mineral structures and for the disclosure of complex polytypic systems. Moreover, the systematic application of this technique may significantly contribute to the discovery of new mineral species, previously undetected due to their small crystal size or complex paragenesis. This may impact on the estimation of rarity in mineralogy [88], and may possibly help in filling the gap between the number of mineral species estimated by “mineral ecology” [89] and the number of minerals actually observed, which seems to be highly underestimated for 15 geochemical elements, among which Al, C, Mg and Na [90, 91]. Additionally, the implementation of refinement procedures that account for dynamical scattering [34–36] allows obtaining fine details on atom coordination and bond distances, and to localizing light atoms, down to hydrogen, at room temperature and for not deuterated samples. On the other hand, due to computational issues dynamical refinement is currently limited to relatively small structures, and cannot be applied for intrinsically disordered materials,

like vaterite [50–52] or denisovite [32]. Indeed, disorder is often a crucial part of nanocrystalline structures, as surface features and defects may concern an important fraction of the diffracting volume.

EDT can open a new scenario also for experimental petrology, where a number of experiments are generally kept hidden in the drawers because standard microprobe and X-ray diffraction data cannot be effectively interpreted. So far, three new phases have been discovered (HAPY [62], HYSO and 11.5 Å phase [38]) and fully crystallographically described. The concurrence of a laboratory specialized in high-pressure syntheses and a dedicated TEM-EDT facility can provide in the next future the ideal experimental set-up for the systematic discovery of new high-pressure phases, which in turn may open new windows on subduction and mantle processes. Another very promising field of investigation concerns micrometeorites, whose mineralogical analysis by standard X-ray diffraction techniques is hampered due to the reduced amount of available sample and the typically small grain size, consequence of a fast formation under not-equilibrated conditions.

It is worth stressing that EDT is a quite robust and portable technique: we have obtained comparable results on TEM of three different manufacturers (FEI, ZEISS, JEOL) working at three different acceleration voltages in different electron optical configurations (nano-beam diffraction, nano-diffraction with Köhler illumination, selected-area diffraction). At present, some limiting factors for EDT lie anyway in the design of TEM, evidently supposed to be used as a microscope rather than a diffractometer. The lens system does not always allow an easy configuration with optimal beam conditions, i.e. mild illumination and parallel beam. Intermediate and projector lenses may introduce astigmatism that reduces the accuracy in cell parameter determination and may compromise reflection indexing at high angle. The goniometer rotation may not be smooth or accurate enough, so that during the acquisition the crystal has to be re-centered several times.

Another important limit concerns the deterioration of the sample during the diffraction experiment. Even if EDT requires a much milder illumination than imaging, still beam damage can be critical for some classes of materials. A major improvement derived by the recent introduction of ultra-fast background-free single-electron detectors, which allow for extremely low-dose illumination conditions and fast exposition time [92]. However, materials, where water molecules are an essential part of the crystalline structure, may just undergo amorphization or structure modification in the moment they are inserted inside the TEM vacuum (normally about  $10^{-10}$ – $10^{-11}$  bar). The observation of these materials requires their isolation

from vacuum by the encapsulation in amorphous ice with cryo-plunging and cryo-transfer procedures normally in use for biologic samples.

In conclusion, EDT can be considered a reliable technique for addressing crystallographic questions, every time the complex nature of the sample calls for a single-crystal data collection on grains smaller than few microns. In fact, we believe there are many mineralogical and petrological open problems that would greatly benefit from such approach and the four cases highlighted in this paper, spanning from experimental petrology to rare minerals and phase intergrowths, are far from being exhaustive.

**Acknowledgements:** Authors thank all people that cooperate with them in the analysis of the materials cited in this paper and Luca Bindi for inviting them to contribute to this special issue for *Zeitschrift für Kristallographie*.

## References

- [1] M. Knoll, E. Ruska, *Z. Phys.* **1932**, 78, 318.
- [2] C. Davisson, L. H. Germer, *Phys. Rev.* **1927**, 30, 705.
- [3] R. Rigamonti, *Gazz. Chim. Ital.* **1936**, 66, 174.
- [4] J. M. Cowley, *Acta Crystallogr.* **1956**, 9, 391.
- [5] J. M. Cowley, A. F. Moodie, *Acta Crystallogr.* **1957**, 10, 609.
- [6] H. Bethe, *Ann. Phys.* **1928**, 392, 55.
- [7] M. Blackman, *Proc. R. Soc. Lond. A* **1939**, 173, 68.
- [8] K. Gjønnes, Y. Cheng, B. S. Berg, V. Hansen, *Acta Crystallogr. A* **1998**, 54, 102.
- [9] T. E. Weirich, X. Zou, R. Ramlau, A. Simon, G. L. Casciarano, C. Giacomazzo, S. Hovmöller, *Acta Crystallogr. A* **2000**, 56, 29.
- [10] Z. G. Pinsker (eds.), *Electron Diffraction*, Butterworth, London, **1953**.
- [11] B. K. Vainshtein, *Structure Analysis by Electron Diffraction*, Pergamon Press, Oxford, **1964**.
- [12] A. P. Zhukhlistov, A. S. Avilov, D. Ferraris, B. B. Zvyagin, V. P. Plotnikov, *Crystallogr. Rep.* **1997**, 42, 774.
- [13] D. L. Dorset, H. A. Hauptman, *Ultramicroscopy* **1976**, 1, 195.
- [14] D. L. Dorset, *Acta Crystallogr. B* **1996**, 52, 753.
- [15] T. E. Weirich, *Acta Crystallogr. A* **2001**, 57, 183.
- [16] S. Nicolopoulos, J. M. González-Calbet, M. Vallet-Regí, A. Corma, C. Corell, J. M. Guil, J. Pérez-Pariente, *J. Am. Chem. Soc.* **1995**, 117, 8947.
- [17] I. G. Voigt-Martin, Z. X. Zhang, U. Kolb, C. Gilmore, *Ultramicroscopy* **1997**, 68, 43.
- [18] M. Gemmi, L. Righi, G. Calestani, A. Migliori, A. Speghini, M. Santarosa, M. Bettinelli, *Ultramicroscopy* **2000**, 84, 133.
- [19] R. Vincent, P. A. Midgley, *Ultramicroscopy* **1994**, 53, 271.
- [20] M. Gemmi, X. Zou, S. Hovmöller, A. Migliori, M. Vennström, Y. Andersson, *Acta Crystallogr. A* **2003**, 59, 117.
- [21] D. L. Dorset, C. J. Gilmore, J. L. Jorda, S. Nicolopoulos, *Ultramicroscopy* **2007**, 107, 462.
- [22] M. Gemmi, S. Nicolopoulos, *Ultramicroscopy* **2007**, 107, 483.

- [23] U. Kolb, T. Gorelik, C. Kübel, M. T. Otten, D. Hubert, *Ultra-microscopy* **2007**, 107, 507.
- [24] U. Kolb, T. Gorelik, M. T. Otten, *Ultramicroscopy* **2008**, 108, 763.
- [25] E. Mugnaioli, T. Gorelik, U. Kolb, *Ultramicroscopy* **2009**, 109, 758.
- [26] U. Kolb, E. Mugnaioli, T. E. Gorelik, *Cryst. Res. Technol.* **2011**, 46, 542.
- [27] E. Mugnaioli, *Rend. Fis. Acc. Lincei* **2015**, 26, 211.
- [28] D. B. Williams, C. B. Carter, *Transmission Electron Microscopy*, Plenum Press, New York, **1996**.
- [29] D. Zhang, P. Oleynikov, S. Hovmöller, X. Zou, *Z. Kristallogr.* **2010**, 225, 94.
- [30] B. L. Nannenga, D. Shi, A. G. W. Leslie, T. Gonen, *Nat. Methods* **2014**, 11, 927.
- [31] M. Gemmi, M. G. I. La Placa, A. S. Galanis, E. F. Rauch, S. Nicolopoulos, *J. Appl. Crystallogr.* **2015**, 48, 718.
- [32] I. V. Rozhdestvenskaya, E. Mugnaioli, M. Schowalter, M. U. Schmidt, M. Czank, W. Depmeier, A. Rosenauer, *IUCr* **2017**, 4, 223.
- [33] E. Mugnaioli, U. Kolb, *Microp. Mesop. Mater.* **2014**, 189, 107.
- [34] L. Palatinus, D. Jacob, P. Cuvillier, M. Klementová, W. Sinkler, L. D. Marks, *Acta Crystallogr. A* **2013**, 69, 171.
- [35] L. Palatinus, V. Petříček, C. A. Corrêa, *Acta Crystallogr. A* **2015**, 71, 235.
- [36] L. Palatinus, C. A. Corrêa, G. Steciuk, D. Jacob, P. Roussel, P. Boullay, M. Klementová, M. Gemmi, J. Kopeček, M. C. Domeneghetti, F. Cámara, V. Petříček, *Acta Crystallogr. B* **2015**, 71, 740.
- [37] D. Jacob, L. Palatinus, P. Cuvillier, H. Leroux, C. Domeneghetti, F. Cámara, *Am. Mineral.* **2013**, 98, 1526.
- [38] M. Gemmi, M. Merlini, L. Palatinus, P. Fumagalli, M. Hanfland, *Am. Mineral.* **2016**, 101, 2645.
- [39] L. Palatinus, P. Brázda, P. Boullay, O. Perez, M. Klementová, S. Petit, V. Eigner, M. Zaarour, S. Mintova, *Science* **2017**, 355, 166.
- [40] I. Rozhdestvenskaya, E. Mugnaioli, M. Czank, W. Depmeier, U. Kolb, A. Reinholdt, T. Weirich, *Mineral. Mag.* **2010**, 74, 159.
- [41] I. V. Rozhdestvenskaya, T. Kogure, E. Abe, V. A. Drits, *Mineral. Mag.* **2009**, 73, 883.
- [42] I. Rozhdestvenskaya, U. Kolb, E. Mugnaioli, A. Reinholdt, T. Weirich, W. Depmeier, M. Czank, *Z. Kristallogr. Suppl.* **2009**, 29, 103.
- [43] I. Rozhdestvenskaya, E. Mugnaioli, M. Czank, W. Depmeier, U. Kolb, S. Merlino, *Mineral. Mag.* **2011**, 75, 2833.
- [44] M. Gemmi, I. Camprostrini, F. Demartin, T. E. Gorelik, C. M. Gramaccioli, *Acta Crystallogr. B* **2012**, 68, 15.
- [45] J. Plášil, L. Palatinus, J. Rohlíček, L. Houdková, M. Klementová, V. Goliáš, P. Škácha, *Am. Mineral.* **2014**, 99, 276.
- [46] F. Colombo, E. Mugnaioli, O. Vallcorba, A. Garcia, A. R. Goñi, J. Rius, *Mineral. Mag.* **2017**, 81, 1191.
- [47] G. C. Capitani, E. Mugnaioli, J. Rius, P. Gentile, T. Catelani, A. Lucotti, U. Kolb, *Am. Mineral.* **2014**, 99, 500.
- [48] G. Ventruti, E. Mugnaioli, G. Capitani, F. Scordari, D. Pinto, A. Lausi, *Phys. Chem. Miner.* **2015**, 42, 651.
- [49] J. Majzlan, L. Palatinus, J. Plášil, *Eur. J. Mineral.* **2016**, 28, 63.
- [50] E. Mugnaioli, I. Andrusenko, T. Schüler, N. Loges, R. E. Dinnebier, M. Panthöfer, W. Tremel, U. Kolb, *Angew. Chem. Int. Ed.* **2012**, 51, 7041.
- [51] E. Makovicky, *Am. Mineral.* **2016**, 101, 1636.
- [52] A. G. Christy, *Cryst. Growth Des.* **2017**, 17, 3567.
- [53] L. Palatinus, M. Klementová, V. Dřínek, M. Jarošová, V. Petříček, *Inorg. Chem.* **2011**, 50, 3743.
- [54] P. Boullay, L. Palatinus, N. Barrier, *Inorg. Chem.* **2013**, 52, 6127.
- [55] L. Bindi, J. M. Eiler, Y. Guan, L. S. Hollister, G. MacPherson, P. J. Steinhardt, N. Yao, *Proc. Natl. Acad. Sci. USA* **2012**, 109, 1396.
- [56] M. Koch-Müller, E. Mugnaioli, D. Rhede, S. Speziale, U. Kolb, R. Wirth, *Am. Mineral.* **2014**, 99, 2405.
- [57] E. F. Rauch, J. Portillo, S. Nicolopoulos, D. Bultreys, S. Rouvimov, P. Moeck, *Z. Kristallogr.* **2010**, 225, 103.
- [58] C. Viti, A. Brogi, D. Liotta, E. Mugnaioli, R. Spiess, A. Dini, M. Zucchi, G. Vannuccini, *J. Struct. Geol.* **2016**, 86, 1.
- [59] I. Pignatelli, Y. Marrocchi, E. Mugnaioli, F. Bourdelle, M. Gounelle, *Geochim. Cosmochim. Acta* **2017**, 209, 106.
- [60] I. Pignatelli, E. Mugnaioli, J. Hybler, R. Mosser-Ruck, M. Cathelineau, N. Michau, *Clays Clay Miner.* **2013**, 61, 277.
- [61] I. Pignatelli, E. Mugnaioli, R. Mosser-Ruck, O. Barres, U. Kolb, N. Michau, *Eur. J. Mineral.* **2014**, 26, 221.
- [62] M. Gemmi, J. Fischer, M. Merlini, S. Poli, P. Fumagalli, E. Mugnaioli, U. Kolb, *Earth Planet. Sci. Lett.* **2011**, 310, 422.
- [63] S. Bhat, L. Wiehl, L. Molina-Luna, E. Mugnaioli, S. Lauterbach, S. Siculo, P. Kroll, M. Duerrschnabel, N. Nishiyama, U. Kolb, K. Albe, H.-J. Kleebe, R. Riedel, *Chem. Mater.* **2015**, 27, 5907.
- [64] G. C. Capitani, E. Mugnaioli, A. Guastoni, *Am. Mineral.* **2016**, 101, 1679.
- [65] A. Baraldi, E. Buffagni, R. Capelletti, M. Mazzera, M. Fasoli, A. Lauria, F. Moretti, A. Vedda, M. Gemmi, *J. Phys. Chem. C* **2013**, 117, 26831.
- [66] L. Palatinus, *PETS – Program for Analysis of Electron Diffraction Data*, Institute of Physics of the AS CR, Prague, **2011**.
- [67] M. C. Burla, R. Caliendo, B. Carrozzini, G. L. Cascarano, C. Cuocci, C. Giacovazzo, M. Mallamo, A. Mazzone, G. Polidori, *J. Appl. Crystallogr.* **2015**, 48, 306.
- [68] G. M. Sheldrick, *Acta Crystallogr. A* **2008**, 64, 112.
- [69] P. Fumagalli, S. Poli, *J. Petrol.* **2005**, 46, 555.
- [70] P. Fumagalli, S. Poli, J. Fischer, M. Merlini, M. Gemmi, *Contrib. Mineral. Petrol.* **2014**, 167, 979.
- [71] K. Momma, F. Izumi, *J. Appl. Crystallogr.* **2011**, 44, 1272.
- [72] V. Petříček, M. Dušek, L. Palatinus, *Z. Kristallogr.* **2014**, 229, 345.
- [73] M. C. Burla, R. Caliendo, M. Camalli, B. Carrozzini, G. L. Cascarano, L. De Caro, C. Giacovazzo, G. Polidori, D. Siliqi, R. Spagna, *J. Appl. Crystallogr.* **2007**, 40, 609.
- [74] L. Akselrud, Y. Grin, *J. Appl. Crystallogr.* **2014**, 47, 803.
- [75] L. Palatinus, G. Chapuis, *J. Appl. Crystallogr.* **2007**, 40, 451.
- [76] J. Felsche, *J. Appl. Crystallogr.* **1969**, 2, 303.
- [77] A. N. Christensen, A. F. Jensen, B. K. Thomsen, R. G. Hazell, M. Hanfland, E. Dooryhee, *Acta Chem. Scand.* **1997**, 51, 1178.
- [78] V. P. Rogova, Y. P. Rogov, V. A. Drits, N. N. Kuznetsova, *Zapiski Vsesoyuznogo Mineralogicheskogo Obshchestva* **1978**, 107, 94.
- [79] Y. P. Menshikov, *Zapiski Vsesoyuznogo Mineralogicheskogo Obshchestva* **1984**, 113, 718.
- [80] K. Dornberger-Schiff, K. Fichtner, *Krist. Techn.* **1972**, 7, 1035.
- [81] G. Ferraris, E. Makovicky, S. Merlino, *Crystallography of Modular Materials, IUCr Monographs on Crystallography* 15, Oxford University Press, Oxford, **2004**.
- [82] S. V. Krivovichev, *Mineral. Mag.* **2013**, 77, 275.
- [83] E. Mugnaioli, *Acta Crystallogr. B* **2015**, 71, 737.

- [84] C. A. Corrêa, M. Klementová, V. Dřínek, J. Kopeček, L. Palatinus, *J. Alloys Compd.* **2016**, 672, 505.
- [85] M. Colmont, L. Palatinus, M. Huvé, H. Kabbour, S. Saitzek, N. Djelal, P. Roussel, *Inorg. Chem.* **2016**, 55, 2252.
- [86] M. Klementová, M. Karlík, P. Novák, L. Palatinus, *Intermetallics* **2017**, 85, 110.
- [87] E. Mugnaioli, M. Gemmi, M. Merlini, M. Gregorkiewicz, *Acta Crystallogr. B* **2016**, 72, 893.
- [88] R. M. Hazen, J. H. Ausubel, *Am. Mineral.* **2016**, 101, 1245.
- [89] R. M. Hazen, E. S. Grew, R. T. Downs, J. Golden, G. Hystad, *Can. Mineral.* **2015**, 53, 295.
- [90] R. M. Hazen, G. Hystad, R. T. Downs, J. J. Golden, A. J. Pires, E. S. Grew, *Am. Mineral.* **2015**, 100, 2344.
- [91] R. M. Hazen, D. R. Hummer, G. Hystad, R. T. Downs, J. J. Golden, *Am. Mineral.* **2016**, 101, 889.
- [92] I. Nederlof, E. van Genderen, Y.-W. Li, J. P. Abrahams, *Acta Crystallogr. D* **2013**, 69, 1223.

---

**Supplemental Material:** The online version of this article offers supplementary material (<https://doi.org/10.1515/zkri-2017-2130>).